3D numerical design of tunnel hood

David Uystepruyst, Mame J.-P. William-Louis, François Monnoyer de Galland

3D numerical design of tunnel hood

David Uystepruyst[a,b,*], Mame William-Louis[c], François Monnoyer[a,b]

[a] *Université Lille Nord-de-France, F-59000 Lille, France.*
[b] *TEMPO, Université de Valenciennes et du Hainaut-Cambrésis, 59313 Valenciennes Cedex 9, France.*
[c] *Univ. Orléans, ENSI de Bourges, PRISME, EA 4229, F45072, Orléans.*

Abstract

This paper relates to the parametric study of tunnel hoods in order to reduce the shape, i.e the temporal gradient, of the pressure wave generated by the entry of a High speed train in tunnel. This is achieved by using an in-house three-dimensional numerical solver which solves the Eulerian equations on a Cartesian and unstructured mesh. The efficiency of the numerical methodology is demonstrated through comparisons with both experimental data and empirical formula. For the tunnel hood design, three parameters, that can influence the wave shape, are considered: the shape, the section and the length of the hood. The numerical results show, (i) that a constant section hood is the most efficient shape when compared to progressive (elliptic or conical) section hoods, (ii) an optimal ratio between hood's section and tunnel section where the temporal gradient of the pressure wave can be reduced by half, (iii) a significant efficiency of the hood's length in the range of 2 to 8 times the length of the train nose. Finally the influence of the

*Corresponding author at: TEMPO, Université de Valenciennes et du Hainaut-Cambrésis, 59313 Valenciennes Cedex 9, France.

Email address: david.uystepruyst@univ-valenciennes.fr (David Uystepruyst)

train's speed is investigated and results point out that the optimum section is slightly modified by the train's speed.
Keywords:
Computational fluid dynamics, Euler equations, Three-dimensional simulation, High-speed trains, Tunnel hood.

---

1. Introduction

A train entering tunnel generates a compression wave propagating to the opposite portal, where it is partly emitted outside and partly reflected back in the tunnel as a rarefaction wave. The emerging outside part, called the micro-wave, may, in certain circumstances, be strong enough to produce a booming noise up to 140-150 dB. This kind of disturbances can have dramatical effects on the neighborhood environment of the tunnel exit, occurring structural damages and much annoyance.

The magnitude and the duration of those waves are strongly linked to the temporal pressure gradient of the initial compression wave generated by the entry of the train nose in the tunnel. This temporal pressure gradient can be reduced by modifying the wave generation process. This can be achieved by optimizing the shape of the train nose [1, 2, 3, 4, 5] or by adding a progressive entry portal to the tunnel [6, 7, 8, 9, 10]. Indeed, the temporal pressure gradient essentially depends on the train Mach number and the blockage ratio, σ, defined as the ratio of the cross-sectional area of the train to the tunnel entry cross-sectional area. The modifications of the train nose or the addition of a progressive entry allows the evolution of the blockage ratio to

be modified and, therefore, the temporal pressure gradient.

Despite the advances in computer efficiency, the parametric study of a transient three-dimensional physical phenomena remains a challenge, and the existing numerical parametric studies are not exhaustive. The oldest study was performed by SNCF researchers [7]. In this paper, the hood shape and perforations were investigated using only three comparisons. In reference [9] the authors compared nine perforated entries having no section discontinuity between hood and tunnel. The optimal hood leads to a reduction of about 43% of the temporal pressure gradient. The most elaborate study was carried out by Liu *et al.* [10], where a parametric study of the hood section was performed for three hood lengths. The optimal hood section was about 1.8 times the tunnel section for the three hood lengths. Studies of different hood shapes and perforated hoods were carried out as well. However, this study was performed at a low speed of 160 km/h.

The large number of recent works on the optimization of train nose [4, 5], on the investigation of hoods effects [9, 10, 11], or on simple study of train-tunnel entry [12, 13] shows that the problems occurring when trains enter tunnels are still relevant and becomes even more important with the increase of the velocity and the development of high-speed trains in the world.

The main purposes of the present work are to precisely define an optimal hood for a tunnel in which a train is entering at high-speed velocities, higher than 250 km/h, and to thoughtfully describe physical phenomena involved

by different hoods. In order to achieve this, a numerical parametric study of the hood was carried out. The considered parameters were the shape, the section and the length of the hood. This introductory part is followed by a description of the numerical model in section 2. This is followed by a description of the geometrical models used in this study in section 2.3. The capability of the numerical method to correctly reproduce the phenomena is shown in section 3. Afterwards, the hood geometries and the results of the studies of the shape, the section and the length of the hood are provided in section 4.1, 4.2 and 4.3, respectively. In section 4.4, the effect of the train velocity is studied.

2. The numerical model

2.1. Governing equations

When a train enters a tunnel, the pressure forces are strongly dominant as compared to the viscous forces. Therefore, the viscosity was neglected as well as the turbulence of the flow. The simulations were modeled by the three-dimensional equations of conservation of mass, quantity of movement and energy:

$$\partial_t \mathbf{U} + \nabla \cdot \mathbf{H}(\mathbf{U}) = 0, \tag{1}$$

where $\mathbf{U}$ is the vector of conservative variable and $\mathbf{H}(\mathbf{U})$ is the fluxes tensor

:

$$\mathbf{U} = \begin{pmatrix} \rho \\ \rho u \\ \rho v \\ \rho w \\ \rho E \end{pmatrix}, \text{ and } \mathbf{H}(\mathbf{U}) = \begin{pmatrix} \rho u_r & \rho v_r & \rho w_r \\ \rho u u_r + p & \rho u v_r & \rho u w_r \\ \rho v u_r & \rho v v_r + p & \rho v w_r \\ \rho w u_r & \rho w v_r & \rho w w_r + p \\ \rho u_r h_0 + p u_t & \rho v_r h_0 + p v_t & \rho w_r h_0 + p w_t \end{pmatrix}.$$

In the definitions of $\mathbf{U}$ and $\mathbf{H}(\mathbf{U})$, the variables are the density ρ, the energy E, the pressure p and the total enthalpy h_0. u_r, v_r and w_r are the three components of the relative velocity $\mathbf{V}_r$, defined as $\mathbf{V}_r = \mathbf{V} - \mathbf{V}_t$ where $\mathbf{V} = (u, v, w)^t$ is the absolute velocity of the flow and $\mathbf{V}_t = (u_t, v_t, w_t)^t$ is the translation velocity of the grid.

Equation (1) was solved using a finite volume method. It combines the second order Roe scheme [14] for the spatial discretization and the Van Leer predictor-corrector scheme [15] for the time integration. To preserve the monotonous property of the scheme during the passage at the second order, the limiter for non-structured mesh of type Barth and Jespersen [16] was used.

2.2. The numerical domain and boundary conditions

A top view of the numerical domain is represented in figure 1. The overall domain was subdivided in two sub-domains. The first one, the sliding domain, contained the train and was set in motion with the translation velocity $\mathbf{V}_t$. The remaining part of the overall domain contained the tunnel walls and the external domain. This second part stayed motionless during simulations,

the translation velocity $\mathbf{V}_t$ of equation (1) was, hence, equal to zero for its computational cells.

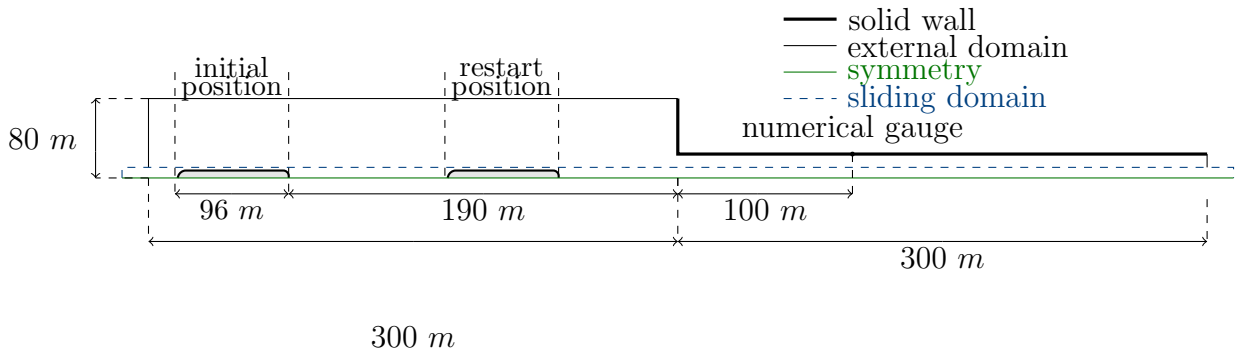

Figure 1: *Numerical domain.*

A solid walls boundary condition was used for the tunnel walls and for the train body. A non reflective boundary condition, based on a Fourier decomposition of the solution at the boundary face [17], was used for the external domain and the tunnel extremity. The cross-sectional section of the train was centered inside the tunnel, a symmetry boundary condition was then used to divide the computational domain by two. A common interface was calculated between the sliding domain and the second domain, and a conservative flux calculation was performed, i.e. at a common interface the flow variables were updated by calculating a flux and not by interpolating, see [17] for more details.

2.3. Geometrical models and numerical details

For this study, the entry of the French TGV, see figure , into a 63 m^2 section area tunnel at a speed of 250 km/h ($M \simeq 0.2$ with $T = 293\ K$),

except for section 4.4, was considered. The geometries of the TGV and the tunnel are shown in figure 2. The blockage ratio σ was 0.152.

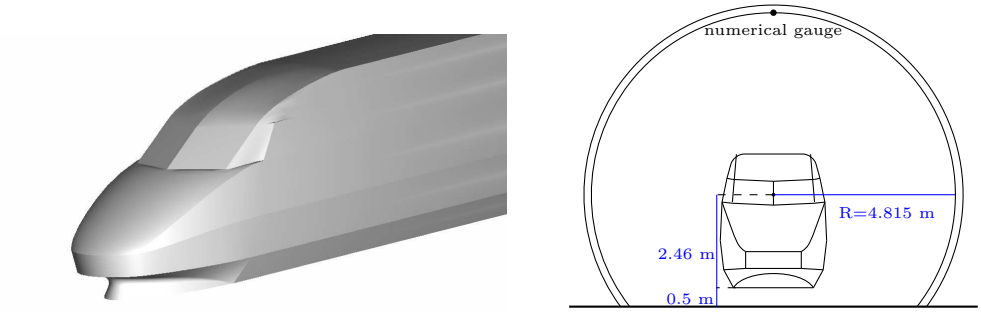

(a) Nose of the TGV (b) Front view of the TGV into the tunnel

Figure 2: *Geometric properties (in m).*

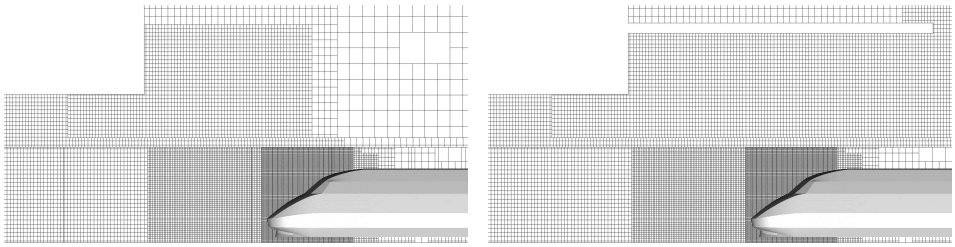

(a) without hood (b) with hood

Figure 3: *Volume mesh on the cut plane* $y = 0$.

The train length was 96 m, hence the rarefaction wave generated by the rear train entry did not affect the pressure signal recorded by a numerical sensor located 100 m after the tunnel entry.

The computational grid was performed by an automatic grid generator which made Cartesian volume mesh based on a triangular surface mesh. The grid

generator used an Octree structure which means, in particular, that the size ratio between two neighbor computational cells cannot be different to one or two. A cut plane view of the volume mesh is shown in figure 3 for the configuration without hood and for one configuration with hood. The overall domain contained between 1.250.000 and 1.350.000 elements. As can be seen in figure 3, the fine mesh at the tunnel entry, in figure 3(a), is extended inside the hood, 3(b). Therefore, the number of elements evolves according to the size (length and/or section) of the hood. The minimum mesh size was located on the train nose, as can be seen in both figures 3(a) and 3(b), and was about 0.05 m. For the train sub-domain, i.e. the sliding sub-domain in figure 1, the mesh size grew to 0.1 m, and then 0.2 m in front of the train. A fine mesh was required in front of the train for the good simulation of the compression wave. Others sub-domains were finely meshed into the hood and into the tunnel, as shown in figures 3(a) and 3(b). where the minimal space discretization is 0.2 m. The time-step was $\Delta t = 3.4 \times 10^{-5}$ s.

3. Validation

3.1. Tunnel without hood

First, the reference configuration described in section 2.3 had to be validated. Unfortunately, experimental data were not available for this configuration. Nevertheless, it was possible to determine the maximum value of pressure, as well as the maximum value of pressure gradient, with empirical formula. These formula depend on parameters which can be determined by experimental measurements. Some previous experimental measurements were available such the case of the TGV running in the Villejuste tunnel

	ΔP max		$\partial P/\partial t$ max	
	value (Pa)	diff./ref. (%)	value (Pa/s)	diff./ref. (%)
Experimental	1281		8400	
Numerical	1251	-2	8795	+4

Table 1: *Experimental data and numerical results of the maxima of pressure and pressure gradient for the entrance of the TGV in the Villejuste tunnel [18].* $V = 220\ km/h$, $\sigma = 0.21$.

[18]. As soon as the parameters were determined, it was possible to estimate the maximum values of both pressure and pressure gradient for the reference configuration of the present parametric study.

The Villejuste tunnel located on the high-speed southwest line in France, has a section of 46 m^2, giving a blockage ratio of 0.21. The velocity of the TGV was 220 km/h [18].

The experimental data and the numerical results of the pressure rise and the maximum of pressure gradient are presented in table 1. It is shown that the numerical methodology gives results in good convenience with experimental data.

These maxima can be also estimated by formula developed by Pope [19], also presented in [20], for the pressure rise:

$$\Delta p = \gamma p_0 M \left[1 + \frac{1 - \sqrt{1 + 2Y}}{Y}\right], \tag{2}$$

where $Y = Mk_n(R^2-1)$ with $k_n = 1+\dfrac{\xi_n}{1-(1-\sigma)^2}$ and $R = \dfrac{1}{1-\sigma}$. M is the train Mach number, p_0 is the free pressure and ξ_n is pressure loss coefficient of the train nose;

Or by the formula of Ozawa [21] for the pressure and the pressure gradient:

$$\Delta p = \frac{\rho}{2} V^2 f(M,\sigma), \tag{3}$$

$$(\partial_t p)_{max} = \eta \frac{\rho}{2} V^3 f(M,\sigma) \frac{1}{d_{tun}}, \tag{4}$$

with

$$f(M,\sigma) = \frac{1-(1-\sigma)^2}{(1-M)\,(M+(1-\sigma)^2)},$$

where ρ is the density, V is the train velocity, d_{tun} is the hydraulic diameter of the tunnel and η is a coefficient depending of the train and the tunnel.

For the following parametric study, the pressure loss coefficient of the nose train of equation (2) can be estimated from the experimental value of Δp given in table 1. It gives a value of 0.02 for the pressure loss coefficient of the TGV. In the same way, the coefficient η of equation (4) can be approximated to 0.82 with the experimental value of pressure gradient maximum. The knowledge of these coefficients allow to apply the formula (2), (3) and (4) to the configuration described in section 2.3, and used in the following parametric study. The values given by the formula and the numerical results are compared in table 2, for the pressure and the pressure gradient.

The numerical values are in good agreement with the formula values. The

	Ozawa	Pope	Numerical
ΔP (Pa)	1113	1126	1144
$\partial_t P$ max (Pa/s)	7082		7522

Table 2: *Formula values and numerical results of the maxima of pressure and pressure gradient for the entrance of the TGV in the* 63 m^2 *section area tunnel.* $V = 250$ km/h, $\sigma = 0.152$.

difference is only 3% for the pressure rise and 6% for the maximum of pressure gradient. As said previously, the coefficient η depends especially on the tunnel entry and can be slightly different for the 63 m^2 tunnel compared to the value obtained for the Villejuste tunnel. This slight discrepancy can explain the low value of pressure gradient given by the formula (4).

3.2. Tunnel with hood

Here, comparisons are performed with the experimental data obtained by Bellenoue et al [22]. In this experimental work, a reduced scale train of 600 mm in length was used. This train was a cylinder of 25 mm in diameter with an elliptic shape nose of 40 mm in length and a flat tail. The tunnel, as the hood, was a cylinder. The inner diameter of the tunnel was 44 mm giving a blockage ratio train/tunnel of $\sigma = 0.32$. In [22], several hood sections, as well as several hood lengths were studied. For the present comparison, the selected hood was such that the ratio between the hood section and the tunnel section was $S_h/S_{tun} = 1.7$, and its length was four times the length of the train nose $L_h = 4L_{nose}$. The velocity of the train was 43 $m.s^{-1}$.

Figure 4 shows the comparisons, for the pressure and the pressure gradient, between the experimental data of [22] and the numerical results. For conve-

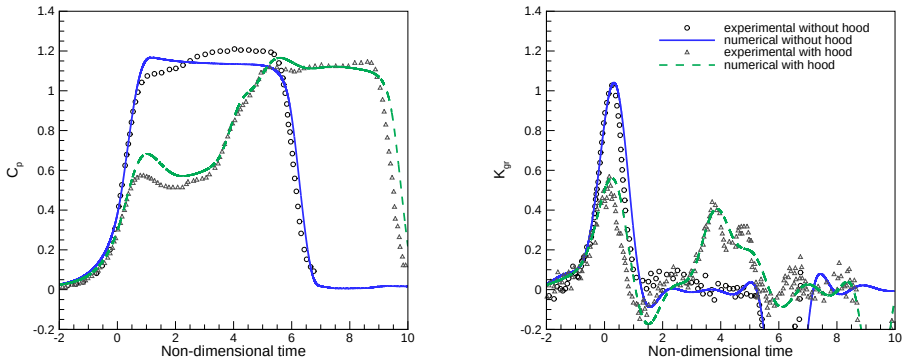

(a) pressure (b) pressure gradient

Figure 4: *Temporal history of the pressure and its gradient. Experimental data from [22], and numerical results.* $V = 43\ m.s{-}1$, $\sigma = 0.32$, $S_h/S_{tun} = 1.7$ *and* $L_h = 4L_{nose}$.

nience, the pressure, the pressure gradient and the time are presented by non-dimensional coefficients, as in the experimental work. The non-dimensional pressure C_p, pressure gradient K_{gr} and time t_a are, then, given by:

$$C_p = \frac{p - p_0}{\frac{1}{2}\rho V^2},\ K_{gr} = \frac{\partial_t p}{\frac{1}{2}\rho \frac{V^3}{d_{tun}}} \text{ and } t_a = \frac{V(t - t_c)}{L_{nose}} \text{ with } t_c = (L_h + X_{sensor})/c,$$

where c is the sound speed, t_c is then the time needed by the pressure wave to reach the gauge located at distance X_{nose} from the tunnel entrance.

It is shown that the convenience between both approaches is rather good. The maxima values of the pressure gradients are, especially, well determined by the numerical methodology. Moreover, it is shown that the numerical methodology is suitable to reproduce main phenomena : compression waves, rarefaction wave, etc.

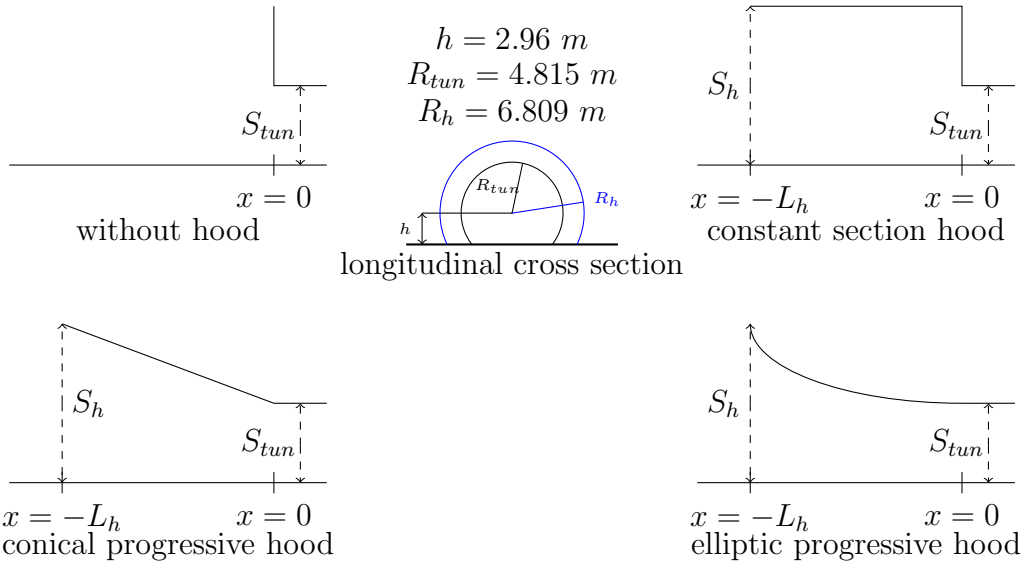

Figure 5: *Hood shape.*

4. Results

4.1. Hood shape

4.1.1. The test layout

In order to highlight the effect of the hood shape, four cases were simulated, see figure 5. The first one concerned a tunnel without a hood, and is considered as the reference for all other calculations. The second one was a hood with a constant section, and the two last were progressive hoods with a section progressively reducing to that of the tunnel. This progressive evolution was conical for the third configuration and elliptical for the last. For this study, the hood length, L_h, was fixed at 20 m and the hood section, S_h, is 1.775 times the tunnel section, S_{tun}. The tunnel and hood cross sections are two concentric circles truncated by the ground with hood radius defined as $R_h = \sqrt{2}R_{tun}$, see figure 5.

4.1.2. Results

Figure 6 shows the temporal evolution of the pressure, recorded at 100 m from the tunnel entry, and its temporal gradient. On these graphs, the time $t = 0\ s$ is the train/tunnel entry instant.

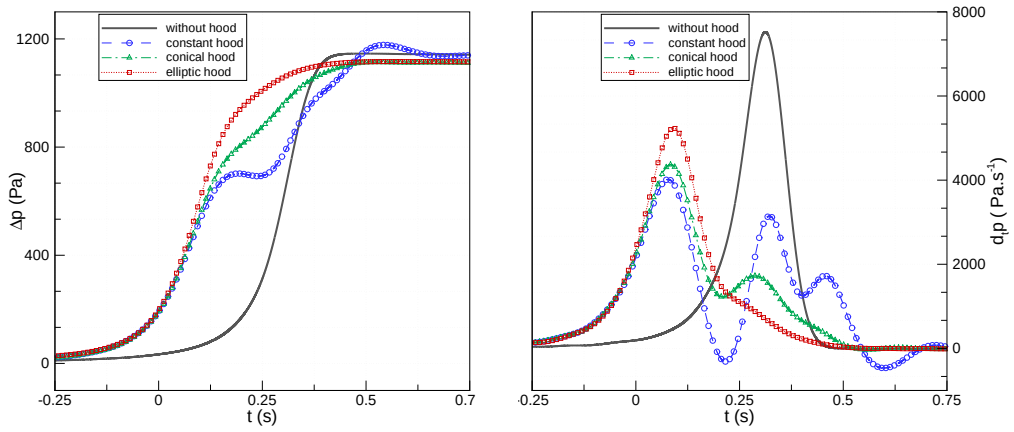

(a) pressure (b) pressure gradient

Figure 6: *Temporal history of the pressure and its gradient. Numerical results obtained on the four hood shapes defined in 5.* $V = 250\ km/h$, $\sigma = 0.152$, $S_h/S_{tun} = 1.775$ *and* $L_h = 20\ m$.

The configuration without a hood clearly produces a single jump in pressure. It is also clear that configurations with hoods considerably reduce the pressure gradient. Both progressive hoods imply a substantial pressure increase at first which corresponds to the entry of the train in the hood. This substantial increase leads to a first peak of gradient. During a second phase, the pressure increases slowly due to the narrowing of the hood section and, therefore the rise of the train-hood blockage ratio.

The elliptic hood yield an important first pressure jump, involving a pressure gradient maximum of 5326 Pa/s, see table 3. The decrease of its cross-sectional area was faster than that of the conical hood, see figure 5. That means at the same time, the blockage ratio with the conical hood was, then, higher and, finally, the pressure, as well as the pressure gradient, was higher. For the conical hood, the changes in cross-sectional area were more important at the end of the hood, this yields a second pressure jump before the train entered the tunnel around time $t = 0.25\ s$, see figure 6. As the maximum value of pressure gradient was 4368 Pa/s, it can be concluded that the conical hood was more efficient than the elliptical hood. However, as it was shown by Ogawa and Fujii [23] for the train noses, a hood with shape made by a combination of elliptical, conical or even paraboloidal shape could be more efficient.

The constant hood generates a more complex pressure signal. In order to have a better understanding of this pressure evolution, reference may be made to the wave diagram in figure 7.

The *x-axis* of this diagram (bottom of figure 7) is time, and is the same range as the pressure and gradient signals (top of figure 7). The time $t = 0\ s$ corresponds to the train's entry in the tunnel. The $y - axis$ corresponds to the distance traveled in the hood and the tunnel. The distance $d = -20\ m$ is the hood entry, $d = 0\ m$ is the tunnel entry and $d = 100\ m$ is the location of the pressure gauge. Finally, the slanting line is the train nose path inside the hood and the tunnel.

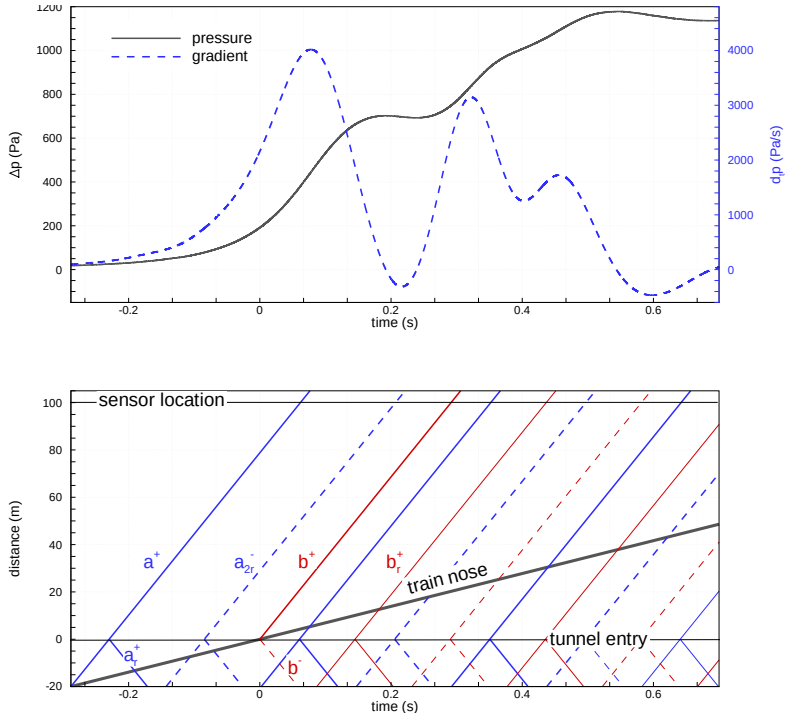

Figure 7: *Wave diagram of the constant hood.* $V = 250\ km/h$, $\sigma = 0.152$, $S_h/S_{tun} = 1.775$ *and* $L_h = 20\ m$.

When the train enters the hood ($t \simeq -0.288\ s$ and $d = -20\ m$), it generates a compression wave a^+ which reaches the sensor at time $t = 0.05\ s$, thereby generating the first peak. Before that, this wave arrives at the tunnel entry where it is partly reflected, producing compression wave a_r^+, on the wall corresponding to the section discontinuity between hood and tunnel. Wave a_r^+ propagates through the hood back towards its entry where it is partly emitted outside and partly reflected back into the hood as rarefaction wave a_{2r}^-. This reflection is not instantaneous due to the generation of transversal waves at corners [24]. Therefore, the reflection delay can be approximated by

	ΔP max		$\partial P/\partial t$ max	
	value (Pa)	diff./ref. (%)	value (Pa/s)	diff./ref. (%)
without hood	1144		7522	
constant section hood	1177	+3	4018	-46
conical progressive hood	1113	-3	4368	-42
elliptical progressive hood	1116	-3	5326	-30

Table 3: *Shape hood maxima pressure amplitude and gradient. Numerical results obtained on the four hood shapes defined in 5.* $V = 250\ km/h$, $\sigma = 0.152$, $S_h/S_{tun} = 1.775$ *and* $L_h = 20\ m$.

the time that the sound travels the hydraulic diameter of the section defined as the difference between hood section and train section. This rarefaction wave reaches the sensor just after time $t = 0.2\ s$, inducing the pressure decrease and the negative gradient.

When the train enters the tunnel ($t = 0\ s$ and $d = 0\ m$), it generates a compression wave b^+ inside the tunnel and a rarefaction wave b^- inside the hood [25]. The compression wave generates the second pressure jump and is immediately followed by another compression wave b_r^+ resulting from the reflection of b^- at the hood entry. The third jump, caused by b_r^+, explains the overestimation of the pressure amplitude generated by the constant section hood in comparison to the reference case.

The elliptic progressive hood gives a reduction of about only 30% on the pressure gradient (Table 3), while with the conical progressive hood, a gain of

42% is obtained. The most efficient hood is the one with a constant section, which leads to a 46% reduction. These last two hoods have quasi equivalent results. However, constant section hood implies a more sophisticated pressure signal and, especially, it allow a rarefaction wave to pass between both main compression waves. For this reason the constant section hood is considered for the following studies.

It is clear that the hood section is primordial in determining the intensity of the first jump in pressure gradient. Namely, a small hood section produces a substantial first jump and, in contrast, a large hood section implies a small first jump. This first jump allows the air inside the tunnel to be made to move. This flow velocity is proportional to the intensity of the first jump, and determines the intensity of the second jump. Therefore, a small hood section leads to a high air velocity in the tunnel and it implies a second jump of low intensity. On the contrary, a large hood section generates low air velocity and substantial second jump. In order to obtain the optimal section leading to the "equalization" of both pressure gradient maxima, a parametric study of the hood section was performed.

4.2. Hood section

4.2.1. The test layout

In order to determine the optimal hood section, 11 calculations were performed with different sections. Hood sections ranged from the smallest R1, with a hood/tunnel ratio of 1.397, to the largest R11, with a hood/tunnel ratio of 3.203. The ratio hood/tunnel is indicated in table 4 for each configuration. Case R0 taken as the reference consists of a tunnel without a

hood.

4.2.2. Results

Figure 6 shows the temporal evolution of the pressure, recorded at the numerical sensor, and its gradient.

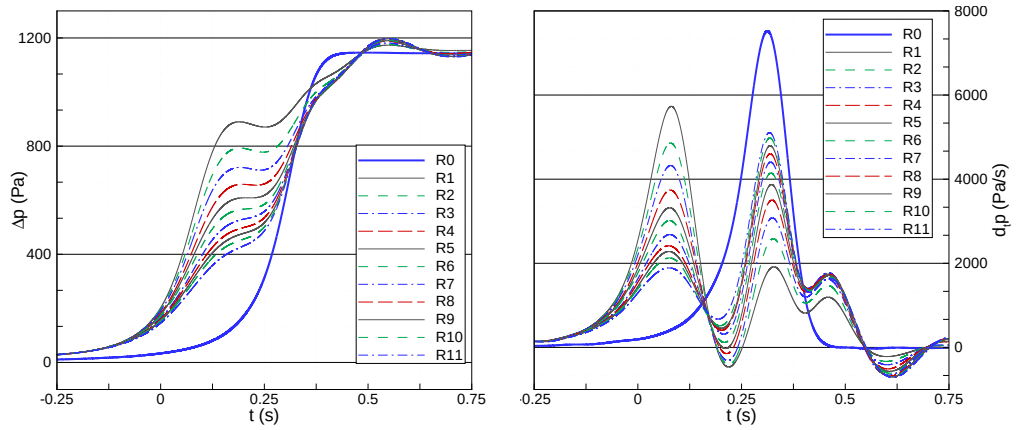

(a) pressure (b) pressure gradient

Figure 8: *Temporal history of the pressure and its gradient. Numerical results obtained on the eleven hood sections.* $V = 250\ km/h$, $\sigma = 0.152$ *and* $L_h = 20\ m$.

It can be seen that configuration R1, with the smallest hood section, implies the largest first pressure jump. This jump diminishes when the section increases, and it is minimal for the largest section R11. In contrast, the second pressure jump is minimized by configuration R1, and this second pressure jump increases with the hood section becoming maximal for configuration R11. The third pressure jump increases likewise in accordance with the hood section. Indeed, this third pressure jump is caused by the reflection of the rarefaction wave generated, in the hood, by the train's entry in the tunnel.

	S_{hood}/S_{tunnel}	$\Delta p(Pa)$	diff./R0. (%)	$\partial P/\partial t$ max (Pa/s)	diff./R0. (%)
R0	1	1144	0	7522	0
R1	1.397	1173	+2,5	5732	-24
R2	1.588	1176	+2,8	4857	-35
R3	1.775	1178	+3	4326	-47
R4	1.959	1188	+3,8	3740	-50
R5	2.142	1190	+4	3873	-48
R6	2.322	1192	+4,2	4145	-45
R7	2.501	1197	+4,6	4407	-41
R8	2.678	1197	+4,6	4603	-39
R9	2.854	1197	+4,6	4796	-36
R10	3.029	1198	+4,7	4978	-34
R11	3.203	1198	+4,7	5105	-32

Table 4: *Pressure magnitude and pressure gradient maxima. Numerical results obtained on the eleven hood sections.* $V = 250\ km/h$, $\sigma = 0.152$ *and* $L_h = 20\ m$.

This third jump is, therefore, proportional to the second jump. Graphically, the most efficient hood, with the best "equalization" of both main jumps, is shown to be configuration R4, with a ratio $S_h/S_{tun} = 1.959$.

This is confirmed by the values of pressure magnitude and pressure gradient maxima given in Table 4. Configuration R4 is the most efficient, with a reduction of about 50% in the temporal pressure gradient. Note that the pressure magnitude increases with the hood section as the third pressure jump increases.

Figure 9 shows the evolution of the pressure gradient maxima in figure 9(a) and the evolution of both the main jumps in figure 9(b) with the ratio S_h/S_{tun}.

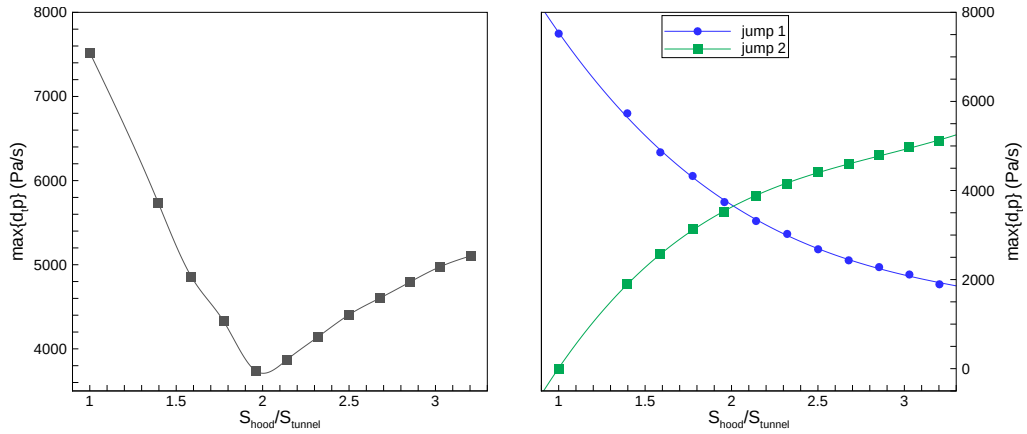

(a) global (b) two main jumps

Figure 9: *Maxima temporal pressure gradient evolution. Numerical results obtained on the eleven hood sections.* $V = 250\ km/h$, $\sigma = 0.152$ *and* $L_h = 20\ m$.

The optimal section is given by the minimal value on the first graph 9(a) or by the intersection of both curves on the second graph 9(b). The section obtained corresponds to the section defined by $S_h \simeq 2Stun$.

4.3. Hood length

4.3.1. The test layout

In this part, 10 calculations were performed with a hood length dimensioned by the length of the train nose which is an important parameter in the wave

generation process. Equation (5) summarizes the ten configurations:

$$\begin{cases} (L_h)_1 = \dfrac{L_{nose}}{2} = 3\ m \\ (L_h)_i = (i-1)L_{nose}, \ \text{for } i = 2, \ldots, 10. \end{cases} \tag{5}$$

The hood section is the optimal section found in the previous section.

4.3.2. Results

Figure 10 shows the temporal evolution of the pressure, recorded at the numerical sensor, and its gradient. Configuration L0 refers to reference calculation without hood.

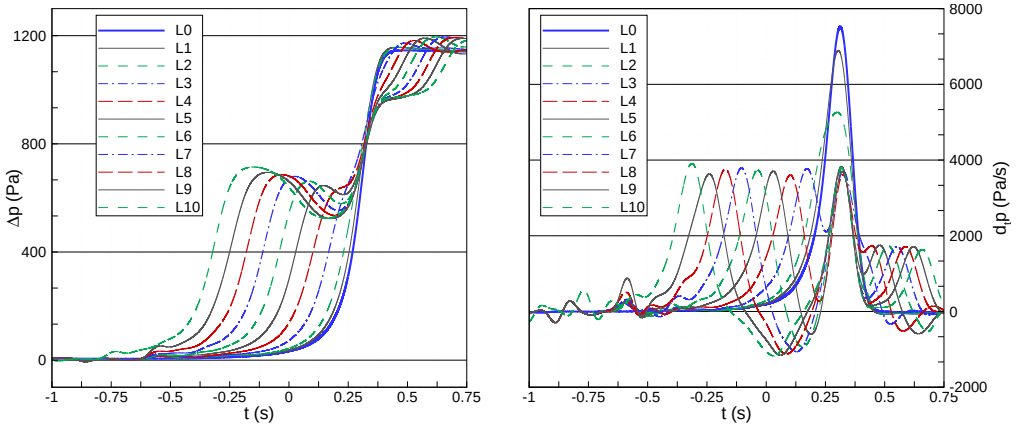

(a) pressure (b) pressure gradient

Figure 10: *Temporal history of the pressure and its gradient. Numerical results obtained on the ten hood lengths defined in equation (5). $V = 250\ km/h$, $\sigma = 0.152$ and $S_h/S_{tun} = 2$.*

As the time $t = 0\ s$ corresponds to the train's entry in the tunnel, the first pressure jump is shifted in time: the longest hoods generates the earliest jumps and also the most substantial pressure amplitudes. Actually, a long hood leaves more time for wave propagation. Similarly, the rarefaction wave

	$\Delta p(Pa)$	diff./L0. (%)	$\partial P/\partial t$ max (Pa/s)	diff./L0. (%)
L0	1144	0	7522	0
L1	1157	+1,1	6897	-8
L2	1157	+1,1	5263	-30
L3	1173	+2,5	3772	-50
L4	1182	+3,3	3612	-52
L5	1191	+4,1	3708	-51
L6	1196	+4,5	3791	-50
L7	1195	+4,5	3810	-49
L8	1194	+4,4	3825	-49
L9	1190	+4	3830	-49
L10	1184	+3,5	3910	-48

Table 5: *Pressure magnitude and pressure gradient maxima. Numerical results obtained on the ten hood lengths defined in equation (5).* $V = 250\ km/h$, $\sigma = 0.152$ *and* $S_h/S_{tun} = 2$.

has a greater amplitude when the hood is longer. The second compression wave occurs at the same time for all configurations; indeed, it is generated by the train's entry in the tunnel. The last compression wave, generated by the rarefaction wave induced by the tunnel entry reflection, is delayed in time. The two shortest hoods imply pressure signals near to that of the un-hooded signal. This is confirmed by the pressure gradient. Indeed, the two shortest hoods lead to a lower gain than the others hoods. From configuration L3 to configuration L10, both principle compression waves seem to be equivalent. However, a long hood implies greater fluctuations.

Table 5 summarizes the maxima of pressure and pressure gradients. It shows that the optimal hood is L4 (3 times the train's nose length) configuration which leads to 3612 Pa/s. This hood induced an optimal crossing of the rarefaction wave between both main compression waves. A substantial range, between configurations L3 (2 times the train's nose length) and L9 (8 times the train's nose length) leads to a gain approaching 50%. Therefore, a common hood length can be considered such that the hood remains optimal for different trains and for different velocities.

The graphs in figure 11 represent the evolution of the pressure gradient maxima 11(a) and the evolution of both main pressure gradient maxima 11(b) versus the non-dimensional hood length L_h/L_{nose}. The range [L3;L9], in which the gain is constant, is clearly highlighted. Configuration L10 generates an increase in the pressure gradient maxima : if the hood is too long, it behaves like a tunnel (steepening of waves).

The effect of the hood section is clearly more important than its length, and it is possible to take a common hood length for different velocities. Indeed, the Mach number of the train plays an important role in the compression wave generation process. It is interesting to study the effect of the train's velocity on the optimal hood section.

4.4. Effect of the train's velocity on the optimal hood section

As said previously, the hood length is not primordial. For a velocity of 250 km/h, a hood length of between 12 m and 48 m gives approximately the same result. This range certainly evolves with the train's velocity, but it can

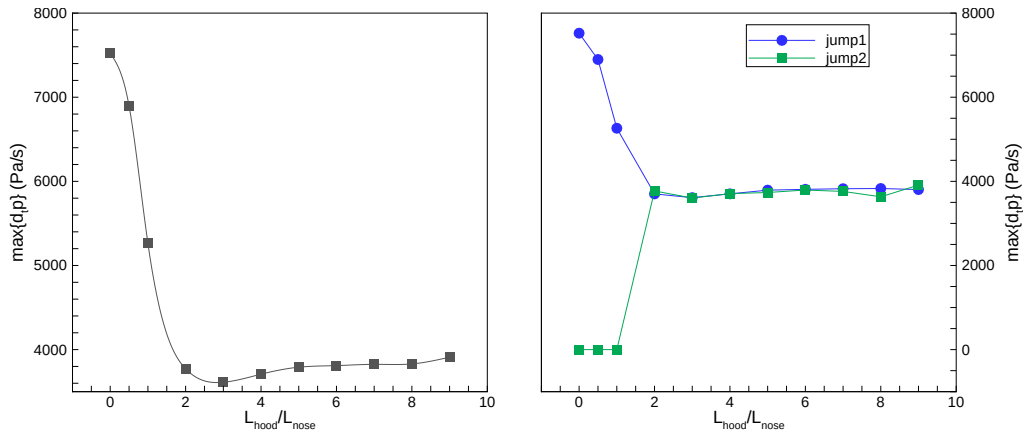

(a) global (b) both main jumps

Figure 11: *Maxima temporal pressure gradient evolution. Numerical results obtained on the ten hood lengths defined in equation 5.* $V = 250\ km/h$, $\sigma = 0.152$ *and* $S_h/S_{tun} = 1.775$.

be supposed that a hood of 20 m in length is in the ideal range for higher velocities. In this study, the hood section is only considered for velocities of 275 km/h, 300 km/h, 325 km/h, 350 km/h and finally 400 km/h. The first two correspond to current high-speed train velocities. With the last three, the rarefaction wave a_{2r}^- of the figure 7 does not pass between both main compression waves. Indeed, if we denote by t_0 the time at which the train enters the hood, the time at which the rarefaction wave reaches the tunnel entry is $t_0 + (3L_h + d)/c$, where d is the hydraulic diameter and c the speed of sound. Whereas the time at which the second compression wave is generated in the tunnel, corresponding to the train's entry, is $t_0 + L_h/Mc$, where M is the train's Mach number. It can easily be seen that when the train's Mach number is over $1/3$, the train reaches the tunnel entry before the rarefaction wave. In this way, it is possible to see the effect of the rarefaction wave on the optimal hood section.

Figure 12 shows the results. The graph on the left represents the evolution of the pressure gradient maxima versus the ratio hood section and tunnel section for all velocities. And the graph on the right is the evolution of the pressure gradient maxima versus the Mach number cube, for the configuration without hood and for the optimal hood section.

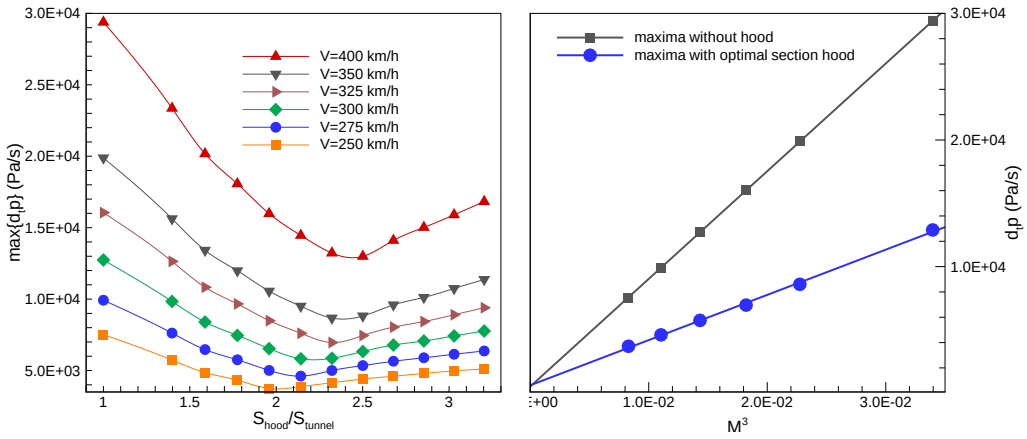

(a) vs. section ratio (b) vs. Mach cube

Figure 12: *Gradient maxima evolution. Numerical results obtained on the eleven hood sections for the six velocities 250 km/h, 275 km/h, 300 km/h, 325 km/h, 350 km/h and 400 km/h.* $\sigma = 0.152$ *and* $L_h = 20$ m.

The graph on the left shows that the optimal ratio S_h/S_{tun} increases with the velocity. However, for the lowest three velocities, corresponding to current velocities, the ratio evolution is weak. The difference between the optimal ratio at $V = 250$ km/h and $V = 300$ km/h is only 10 per cent.

Evolutions of both gradient maxima (without hood and with optimal hood section) versus the cube of the Mach number, graph on the right, are linear.

This is a well-known result without a hood, see equation (4), and as is shown here the maximum of the temporal pressure gradient for the optimal hood can be known by the train's Mach number.

Figure 13 shows the evolution of the optimal hood section versus the Mach number cube inverse.

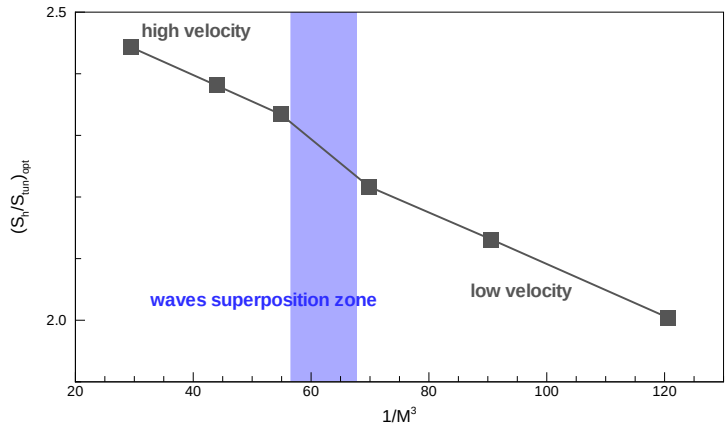

Figure 13: *Optimal section hood evolution versus the Mach number cube inverse. Numerical results obtained on the eleven hood sections for the six velocities 250 km/h, 275 km/h, 300 km/h, 325 km/h, 350 km/h and 400 km/h.* $\sigma = 0.152$ *and* $L_h = 20$ m.

The fact that the optimal section increases with the train's velocity is highlighted. The curve is clearly divided into two linear zones. The first one corresponds to the low velocities, where the rarefaction wave is located between the two main compression waves. The second one is obtained with high velocities, for which the rarefaction wave is behind the second compression wave. The slopes of these two lines are the same. Between these two lines, the sudden jump is recorded when the rarefaction wave and the second

compression wave are superimposed.

5. Conclusion

The effects of tunnel hood on the maximum pressure and the temporal gradient of the pressure were investigated by the help of a well-tested three-dimensional numerical tools. The parametric study dealt with the shape, the cross section and the length of the hoods.

- The comparison of the use respectively of an elliptic, conical and constant evolution of the hood shape, showed that the last configuration was the most efficient. Indeed, a reduction by 46% of the maximum pressure gradient was obtained.

- The effects of the cross section of the hoods showed that the optimal ratio R between the hood section and the tunnel section was about 2: the maximum pressure gradient was reduced by 50% with a R equal to 1.959.

- The influence of the length was characterized by using the ratio between the hood length and the nose length. It was shown that when this ratio increases the maximum pressure gradient decreases and this up to R=2 where the reduction was about 50%. This reduction remained quasi-constant until R=8. Beyond this value, the maximum of pressure gradient increased. This means that when the hood length is greater than 8 times the train nose length, the hood behaves like a tunnel.

Finally, it was shown that the optimal section increases with the train's velocity. It was, in particular, shown that the rarefaction wave a_{2r}^{-} plays an

important role in the determination of the optimal hood section.

A perspective work could be to study the effects of perforated hoods. Indeed, perforations modify the initial compression wave and, hence, could reduced further the disturbances.

References

[1] T. Maeda, T. Matsumura, M. Iida, K. Uchida, Effect of shape of train nose on compression wave generated by train entering tunnel, Proceedings of the International Conference on Speedup Technology for Railway and Maglev Vehicles 2 (1993) 315–319.

[2] T. Ogawa, K. Fujii, Numerical investigation of three-dimensional compressible flows induced by a train moving into a tunnel, Computers & Fluids 26 (1997) 565–585.

[3] M. Bellenoue, T. Kageyama, Train/tunnel geometry effects on the compression wave generated by a high-speed train, Notes on Numerical Fluid Mechanics and Multidisciplinary Design 79 (2002) 276–289.

[4] Y. Ku, J. Rho, S. Yun, M. Kwak, K. Kim, H. Kwon, D. Lee, Optimal cross-sectional area distribution of a high-speed train nose to minimize the tunnel micro-pressure wave, Struct. Multidisc. Optim. 42 (2010) 965–976.

[5] K. Kikuchi, M. Iida, T. Fukuda, Optimization of train nose shape for reducing micro-pressure wave radiated from tunnel exit, Journal of Low Frequency Noise, Vibration and Active Control 30 (2011) 1–19.

[6] M. S. Howe, On the compression wave generated when a high speed train enters a tunnel with a flared portal, Journal of Fluids and Structures 13 (1999) 481–498.

[7] J.-M. Réty, R. Grégoire, Numerical investigation of tunnels extensions attenuating the pressure gradient generated by a train entering a tunnel, Notes on numerical fluid mechanics and multidisciplinary design 79 (2002) 239–248.

[8] M. S. Howe, M. Ida, T. Maeda, Y. Sakuma, Rapid calculation of the compression wave generated by a train entering with a vented hood, Journal of Sound and Vibration 297 (2006) 267–292.

[9] X. Xiang, L. Xue, Tunnel hoods effects on high speed train-tunnel compression wave, Journal of Hydrodynamics 22(5) (2010) 897–904.

[10] T. Liu, H. Tian, X. Liang, Design and optimization of tunnel hoods, Tunnel and Underground Space technology 25 (2010) 212–219.

[11] D. Heine, K. Ehrenfried, Experimental study of the compression-wave generation due to train-tunnel entry, Proceedings of the First International Conference on Railway Technology: Research, Development and Maintenance, Paper 163 (2012).

[12] X. Li, D. Chen, F. Xie, Y. Z, Unsteady simulation for a high-speed train entering a tunnel, Journal of Zhejiang University-Science A 12 (2011) 957–963.

[13] Y. Ko, C. Chen, I. Hoe, S. Wang, Field measurements of aerodynamic

pressures in tunnels induced by high speed trains, Journal of Wind Engineering and Industrial Aerodynamics 100 (2012) 19–29.

[14] P. Roe, Approximate riemann solvers, parameter vectors, and difference schemes, Journal of Computational Physics 43 (1981) 357–372.

[15] B. Van Leer, Towards the ultimate conservative difference scheme v.a. second order sequel to godunov's method, SIAM J. Sci. Stat. Comput. 32 (1979) 101–136.

[16] T. Barth, D. Jespersen, The design and application of upwind schemes on unstructured meshes, AIAA Paper 89-0366 (1989).

[17] D. Uystepruyst, M. William-Louis, E. Creusé, S. Nicaise, F. Monnoyer, Efficient 3D numerical prediction of the pressure wave generated by high-speed trains entering tunnels, Computers & Fluids, 47 (2011) 165–177.

[18] J.-M. Réty, R. Grégoire, Numerical simulation of the pressure wave generated by a train enters a tunnel, TRANSAERO - A European initiative on transient aerodynamics for railway system optimisation, results of the Brite/Euram project Transient aerodynamics for railway system optimisation (2002) 225–238.

[19] C. W. Pope, W. A. Woods, Boundary conditions for the transit of a train through a tunnel with special reference to the entry and exit mesh fraction and the contact surface, Aerodynamics and Ventilation of Vehicles Tunnel (1992) 79–105.

[20] M. J.-P. William-Louis, C. Tournier, A wave signature based for the prediction of pressure transients in railway tunnels, J. of wind engeneering and industrial aerodynamics 93 (2005) 521–531.

[21] S. Ozawa, T. Maeda, Tunnel entrance hoods for reduction of micropressure wave, Quarterly Report of Railway Technical Research Institute 29 (1988).

[22] M. Bellenoue, B. Auvity, T. Kageyama, Blind hood effects on the compression wave generated by a train entering a tunnel, Experimental Thermal and Fluid Science 25 (2001) 397–407.

[23] T. Ogawa, K. Fujii, Prediction and allievation of a booming noise created by a high-speed train moving into a tunnel, Computational Fluids Dynamics (1996) 808–814.

[24] M. J.-P. William-Louis, C. Tournier, Numerical and experimental study of transversal pressure waves at a tube exit, Experimental Thermal ans Fluid Science 28 (2003) 525–532.

[25] M. Iida, Y. Tanaka, K. Kikuchi, T. Fukuda, Pressure waves radiated directly from tunnel portals at train entry or exit, Quarterly report of railway technical research institute 42, 2 (2001) 83–88.